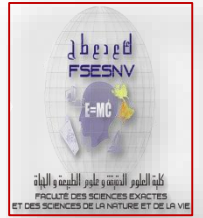Democratic and Popular Republic of Algeria
Ministry of Higher Education and Scientific Research

Echahid Larbi Tebessi University

Faculty of Exact Sciences and Sciences of Life and Nature

Department of Matter Sciences

MASTER'S THESIS

Field: Matter Sciences

Discipline: Physics

Option: Condensed Matter Physics

Theme

Shell model study of the spectroscopic properties of ^{26}Mg

Presented by:

Ali Ammar

Board of Examiners:

Chair:	Boumali Abdelmalek	**Professor**	Larbi Tebessi University
Supervisor:	Bouhelal Mouna	**Professor**	Larbi Tebessi University
Examiner:	Messai Nadjette	**MCB**	Larbi Tebessi University

Date of defence: 24/06/2023

Note: 18.5   **Mention:** Excellent

Democratic and Popular Republic of Algeria

Ministry of Higher Education and Scientific Research

Echahid Larbi Tebessi University

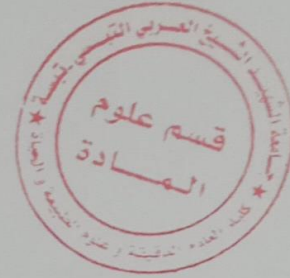Faculty of Exact Sciences and Sciences of Life and Nature

Department of Matter Sciences

MASTER'S THESIS

Field: Matter Sciences

Discipline: Physics

Option: Condensed Matter Physics

Theme

Shell model study of the spectroscopic properties of ^{26}Mg

Presented by:

Ali Ammar

Board of Examiners:

Chair:	Boumali Abdelmalek	Professor	Larbi Tebessi University
Supervisor:	Bouhelal Mouna	Professor	Larbi Tebessi University
Examiner:	Messai Nadjette	MCB	Larbi Tebessi University

Date of defence: 24/06/2023

Note: 18.5

Mention: Excellent

Département de : Sciences de la Matière

Filière : Physique

Spécialité : Physique de la Matière Condensée

Année universitaire 2022/2023

Déclaration sur l'honneur de non-plagiat
(A joindre obligatoirement avec le mémoire)

Je, soussigné(e)

Nom et prénom : Ali Ammar.

Régulièrement inscrit (e) : Mster au département Sciences de la Matière.

N° de carte d'étudiant : Un1201202221066006602.

Année universitaire : 2022/2023.

Domaine : Sciences de la Matière.

Filière : Physique.

Spécialité Physique de la Matière Condensée.

Intitulé : Shell model study of the spectroscopie properteis of ^{26}Mg.

Atteste que mon mémoire est un travail original et que toutes les sources utilisées ont été indiquées dans leur totalité, je certifie également que je n'ai ni copié ni utilisé des idées ou des formulations tirées d'un ouvrage, article ou mémoire, en version imprimée ou électronique, sans mentionner précisément leur origine et que les citations intégrales sont signalées entre guillemets.

Sanctions en cas de plagiat prouvé :

L'étudiant sera convoqué devant le conseil de discipline, les sanctions prévues selon la gravité de plagiat sont :

- L'annulation du mémoire avec possibilité de refaire sur un sujet différent.
- L'exclusion d'une année de Master.
- L'exclusion définitive.

Fait à Tébessa, le :

Signature de l'étudiant (e)

Thesis achieved at

Laboratoire de Physique Appliquée et Théorique LPAT

Acknowledgements

Dedication

We thank God who enabled us to complete this work, and I dedicate this work to everyone who was a reason and support in my academic journey, to all the honorable teachers, my family, friends and colleagues, to everyone who contributed to my education and advice, and to the virtuous Professor Bouhelal Mouna

Abstract

Abstract

The nuclear shell model is a successful model in nuclear physics, and it is one of the important tools for studying nuclear physics. This model is one of the most important theories about the nuclear structure in describing the structure of the nucleus in terms of energy spectra and spectroscopic properties.

The structure of nuclei in the sd shell region has involved many theoretical and experimental studies in analysing and understanding their properties. The well-known USD (or USDA/B) interactions succeeded in describing the properties of normal positive parity states in sd-shell nuclei. The spectroscopic characteristics of the negative parity intruder states as well as the normal positive parity states are well described by the PSDPF interaction.

The aim work of this study is the description of the energy spectrum and spectroscopic properties of the ^{26}Mg nucleus using the PSDPF interaction. The obtained results were compared to available experimental data.

ملخص

ملخص

يعتبر نموذج الطبقات النووية نموذجًا ناجحًا في الفيزياء النووية ، وهو أحد الأدوات المهمة لدراسة الفيزياء النووية. يعتبر هذا النموذج من أهم النظريات حول البنية النووية في وصف بنية النواة من حيث أطياف الطاقة وخصائص التحليل الطيفي.

تضمنت بنية الأنوية في منطقة الطبقة sd العديد من الدراسات النظرية والتجريبية لتحليلها وفهم خصائصها. نجحت التفاعلات المعروفة USD أو (USDA / B) في وصف خصائص حالات التكافؤ الإيجابية العادية في أنوية الطبقة sd يتم وصف الخصائص الطيفية للحالات الدخيلة للتكافؤ السلبي بالإضافة إلى حالات التكافؤ الإيجابي الطبيعي بشكل جيد من خلال تفاعل PSDPF .

الهدف من هذه الدراسة هو وصف طيف الطاقة والخصائص الطيفية لنواة ^{26}Mg باستخدام تفاعل PSDPF ثم مقارنة النتائج التي تم الحصول عليها مع البيانات التجريبية المتوفرة.

Résumé

Résumé

Le modèle en couches nucléaire est un modèle réussi en physique nucléaire, et c'est l'un des outils importants pour étudier la physique nucléaire. Ce modèle est l'une des théories les plus importantes sur la structure nucléaire pour décrire la structure du noyau en termes des spectres d'énergie et des propriétés spectroscopiques.

La structure des noyaux dans la région de la couche sd a impliqué de nombreuses études théoriques et expérimentales dans l'analyse et la compréhension de leurs propriétés. Les interactions bien connues USD (ou USDA/B) ont réussi à décrire les propriétés des états normaux de parité positive dans les noyaux de la couche sd. Les caractéristiques spectroscopiques des états intrus de parité négative ainsi que des états de parité positive normale sont bien décrites par l'interaction PSDPF.

L'objectif de cette étude est la description du spectre en énergie et des propriétés spectroscopiques du noyau ^{26}Mg en utilisant l'interaction PSDPF. Les résultats obtenus ont été comparés aux données expérimentales disponibles.

Table of Contents

Table of contents

List of Tables

List of Figures

X

List of Symbols

Z	Number of protons
N	Number of neutrons
A	Atomic number
$\mathbf{V_{OH}}$	Harmonic-oscillator potential
$\mathbf{H_0}$	The independent movement of nucleons in the nucleus
Ω	The harmonic-Oscillator frequency
$\mathbf{h_i}$	The Hamiltonian of an individual nucleon
$\mathbf{V_{ij}}$	Two-body interaction between the nucleons i and j
$\mathbf{H_r}$	The residual interaction.
$\boldsymbol{E_i}$	Initial state energy
$\boldsymbol{E_f}$	Final state energy
$\boldsymbol{\mu_N}$	The nuclear magneton
$\boldsymbol{\Gamma_\gamma}$	The transition widths
$\boldsymbol{\Gamma_w}$	Weisskopf estimation
$\boldsymbol{\tau_m}$	The mean life time
$\boldsymbol{Y_{LM}}$	Spherical harmonic
EL	Electric
ML	Magnetic transition
e(k)	The nucleon k effective charge
ΔE	The difference in energy
$\boldsymbol{g^l, g^s}$	Gyromagnetic factors of orbit and spin respectively
$\boldsymbol{T_{1/2}}$	Half-life
USD	sd-shell universal interaction compatible with sd valence space
USDA	sd-shell universal interaction compatible with sd valence space (updated version of the USD interaction)
USDB	sd-shell universal interaction compatible with sd valence space (updated version of the USD interaction)

PDSPF	Effective interaction for sd-shell nuclei compatible with p-sd-pf valence space
$0\hbar\omega$	(0 particle-0 hole jump) denotes the positive parity states
$1\hbar\omega$	(1 particle-1 hole jump) denotes the negative parity states

INTRODUCTION

INTRODUCTION

The nuclear shell model is one of the most important nuclear models of the nuclear structure to study the nuclei and determine many nuclear properties (binding energies, spins/parities, electromagnetic decay rates, lifetimes and the nature of electromagnetic transitions, ect.)

Attention was paid to the structure of the nuclei of the sd-shell, whose number of protons Z and of neutrons N is located between the two doubly magic nuclei ^{16}O and ^{40}Ca. This area of nucleiis of primary interest in many experimental and theoretical studies. These nuclei have normal states of positive parity called $0\hbar\omega$ states with a 0 particle - 0 hole configuration, and indruder states with negative parity having a 1 particle - 1 hole configuration, named also $1\hbar\omega$ states. The intruder states result from the excitation of one nucleon between p andsd-shells for nuclei close to ^{16}O or between sd and pf shells for nuclei near ^{40}Ca. For nuclei at the middle of the sd-shell, from Magnesium to Sulphur isotopic chains, their intruder states have a completion between the p-sd or sd-pf excitations. In order to reproduce these states, the model space should be extended to the complete p–sd–pf valence space with a core of ^{4}He. A $(0+1)\hbar\omega$ effective interaction, called PSDPF, compatible with this extensed valence space has been developed by M. BOUHELAL in Strasbourg to ensure a consistent description of both $0\hbar\omega$ and $1\hbar\omega$ states throughout the entire sd-shell.

Know ledge of the level structure of ^{26}Mg (a middle sd-shell nucleus) is crucial for understanding the level structure of its proton-rich mirror nucleus ^{26}Si produced through the thermonuclear ^{25}Al(p,γ)^{26}Si rp-process reaction. The determination of the correct spin/parity assignments of ^{24}Si is necessary to calculate the ^{25}Al(p,γ)^{26}Si reaction rate.

We used the PSDPF interaction to calculate the spectroscopic characteristics of the positive + and negative - parity states of ^{26}Mg and then compared the obtained results with the experimental data. Note that, the calculation was made using the Nathan shell model code developed by E.Caurier in Strasbourg.

The work plan has been divided into three chapters:

- ❖ In chapter I: the nuclear shell model and its useswere presented.
- ❖ In Chapter II: the structure and properties of the sd-shell nuclei, introducing the PSDPF interaction, were presented.
- ❖ In Chapter III: the obtained results were discussed and compared with the experimental data.

Chapter I

Chapter I

Nuclear shell model

The lack of a basic understanding of the nuclear force made it difficult to determine the structure and behaviour of the nucleus. It is not surprising therefore that, instead of a theory, phenomenological models of the nucleus were constructed to accommodate the many remarkable experimental findings [1]. One of the developed models that describe successfully the nuclear structure is the shell model.

In this chapter, we will explain the basic notions of the shell model, which offers the possibility of describing the different characteristics of the nuclei on which the shell model is based.

I.1 Nuclear shell model

Hans Suess and Maria Goeppert Mayer discovered the nuclear shell model in 1949. This model is based on the motion of the individual nucleons, neutrons, and protons. The individual nucleons are considered to be independent particles with independent spins and energy levels, each moving in a potential well produced by the action of all of the other nucleons [2]. The primary evidence for the nuclear shell model was that nuclei with certain specific numbers of protons or neutrons equal to 2, 8, 20, 28, 50, 82, or 126 are particularly stable.

The underlying picture in this model is that each nucleon moves in a mean potential, which is created by its interaction with all the (A-1) other nucleons in the nucleus and is identical for all nucleons. In addition to this mean potential, an extra two-body interaction should be added. The latter depends on a chosen valence space; such as the PSDPF that is an interaction compatible with the p-sd-pf valence space [3].

I.2 Many-body quantum systems

The total energy of N-body quantum system can be acquired as a solution of the time independent Schrödinger equation given by [4]:

$$\hat{H}|\Psi(t)\rangle = \left(\hat{T} + \hat{V}\right)|\Psi(t)\rangle = E|\Psi(t)\rangle \tag{1}$$

Where $\hat{H}$ is composed of the sum of kinetic energy $\hat{T}$ and potential energy $\hat{V}$ operators for the N-body system:

$$\hat{T} = \sum_i^N \left(-\frac{\hbar^2}{2m_i}\nabla^2\right) \tag{2}$$

$$\hat{V} = \sum_{i<j}^N v_{i,j} + \sum_{i<j<k}^N v_{i,j,k} + \sum_{i<j<k<l}^N v_{i,j,k,l} + \cdots \tag{3}$$

Where m_i is the mass of the ith particle in the system, $v_{i,j}$ is the potential between 2-bodies (NN) and $v_{i,j,k}$ for 3-bodies (NNN) etc [4].

The state of $N-$body quantum system is described by its wave function $|\Psi(t)\rangle$.

A common approach used to deal with this many-body problem is by assuming that each interacting body is bound in a static mean-field potential $V(i)$ generated by $N-1$ bodies:

$$\left(\sum_{i=1}^A \left[-\frac{\hbar^2}{2m_i}\nabla_i^2 + V(i)\right] + \left[\hat{V} - \sum_{i=1}^A V(i)\right]\right)|\Psi(t)\rangle = E|\Psi(t)\rangle \tag{3}$$

$$\hat{V}_R|\Psi(t)\rangle = \left(\hat{V} - \sum_{i=1}^N V(i)\right)|\Psi(t)\rangle \tag{4}$$

$$H_0 = \sum_{i=1}^A (t_i + V_i) = \sum_{i=1}^A \left(\frac{P_i^2}{2m} + \frac{1}{2}m\omega^2 r_i^2\right) \tag{5}$$

Where $\hat{H}_0$ is the independent particle Hamiltonian describing individual particles bound in the mean-field potential. The second term, $\hat{V}_R$ is the residual interaction, which contains the leftover N-body interactions, where often only the $2-$body NN interactions are considered. These residual interactions can be treated as perturbations of the mean-field Hamiltonian [4].

I.3 Independent particle shell model

In the beginning of the 20th century, experimental evidence from precision measurements of different nuclear properties indicated a characteristic pattern of enhanced binding energy in nuclei with specific proton and neutron numbers (2,8,20,28,40,50,82,126) so-called 'magic' numbers. The nuclear shell model was developed for describing protons and neutrons bound by the strong nuclear force within the nucleus by similarity with the atomic shell model. In first approximation, the protons and neutrons are described as independent particles bound by each respective mean-field potential (ignoring $\hat{V}_R$ in Eq.I.4) [4].

I.3.1 The Harmonic Oscillator Potential

As a first guess a simple harmonic oscillator potential was used [5]:

$$V_{HO} = \frac{1}{2}m\omega^2 r^2 \tag{6}$$

Where m is the nucleon mass, r is the orbital radius and ω is the angular frequency of the oscillator.

The Schrödinger equation for A nucleons is written as follows:

$$H_0\phi = E_0\phi \tag{7}$$

H_0: The independent movement of nucleons in one body-potential.

Where the Hamiltonian of the independent particles potential is given by

$$\hat{H}_0 = \sum_{i=1}^{A}\left[-\frac{\hbar^2}{2m_i}\nabla_i^2 + V(i)\right] \tag{8}$$

The Eigen functions can be given as:

$$\emptyset_{nlm_l}(r) = R_{nl}(r)Y_l^{ml}(\theta, \varphi) \tag{9}$$

Here l and m_l are the quantum numbers of angular momentum and its oz projection respectively, where as n is the radial quantum number.

Theobtainedsingle-particle energies can be written as [5]:

$$E_l = (N + \frac{3}{2})\hbar\omega = \left(2n + l - \frac{1}{2}\right)\hbar\omega \tag{10}$$

N represents the major number of the harmonic oscillator potential given by:

$$N = 2(n - 1) + l. \tag{11}$$

This potential reproducedonly the first three magic numbers $2, 8, and\ 20$.

I.3.2 Edge-board effect

An improvement was brought by introducing a term representing the "edge-boardeffect"diven by Dl^2 $(D < 0)$[5] to make nucleons at the potential edge more bound. This correction made it possible to remove the degeneracy in l of the solution of Harmonic Oscillator. The Hamiltonian be comes [5]:

$$h_i = t_i + \frac{1}{2}m\omega^2 r_i^2 + Dl_i^2 \qquad (12)$$

The obtained eigen values is given by:

$$E_{nlj}^i = \left(N + \frac{3}{2}\right)\hbar\omega + D(l+1)\hbar^2 \qquad (13)$$

However, here again we do not find the corrects equence of the magic numbers [5]. The inclusion of an attractive orbital angular momentum term l^2 broke the degeneracy of the principal quantum levels and lowered the potential for nucleons with greater angular momentum number. Finally, by adding the contribution from the coupling of orbital angular momentum and the intrinsic spin of the protons and neutrons $s = 1/2$ known as the spin-orbit interaction $\vec{l_i}\vec{s_i}$ resulted in a further broken degeneracy which reproduced the observed magic numbers [3].

I.3.3 Spin-orbit interaction

Only the first three magic numbers were reproduces by the previous Hamiltonian. However, up to now the spin of the nucleons has not been taken into account yet (apart from a factor 2 in determining the magic numbers) [5].

The nucleon-nucleon force has a spin-orbit component, and one can expect that the average single-particle potential also has a spin-orbit part. If $f(r)$ indicates the intensity of the spin-orbit strength, in such a way that the spin-orbit potential has the form [5]:

$$V_{ls} = f(r)\left(\vec{l}.\vec{S}\right) \qquad (14)$$

One can show that $f(r)$ is peaked at the nuclear surface.By the analogy with the electronic case, one often chooses $f(r)$ related to the spin independent part of the average potential in the following way [5]:

$$f(r) = \lambda\frac{1}{r}\frac{dV}{dr} \ ; \lambda \approx -0.5 \ [fm^2] \qquad (15)$$

f(r) is a scalar coefficient for the potential and in principle it depends on l, s and it represents the spin-orbit strength.

The Hamiltonian of a single-particle becomes:

$$h_{i=}t_i + \frac{1}{2}m\omega^2 r_i^2 + Dl_i^2 + f(r)\vec{l_i}\vec{s_i} \qquad (16)$$

The obtained single-particle energies can be written as:

$$E_{nl} = \left(N + \frac{3}{2}\right)\hbar\omega + D(l+1)\hbar^2 + \frac{\hbar^2}{2}\langle f(r)\rangle_{nl} \times \begin{cases} -(l+1) & of \quad j = l - 1/2 \\ l & of \quad j = l + 1/2 \end{cases} \qquad (17)$$

The radial integral $\langle f(r)\rangle_{nl}$ can be represented approximately by the relation [5]:

$$\langle f(r)\rangle_{nl} \approx -20A^{-2/3} MeV \qquad (18)$$

$$\hbar\omega = 41A^{-\frac{1}{3}} \qquad (19)$$

N Is called the major quantum number and in the last step one has rewritten:

n Represents the number on nodes of the radial wave function and can assume values $n = 1; 2; ....$ up o N; l can assume only positive values ($l \geq 0$) up to N and gives the parity of each $N-$th level, which is $(-1)^l$. Taking into account the Pauli principle and spin, the harmonic oscillator energy levels have a large degeneracy, which is given by $(N + 1)(N + 2)$. Each harmonic oscillator level has a large degree of degeneracy that can be written in terms of l [5]:

$$(N + 1)(N + 2) = \sum_l 2(2l + 1) \qquad (20)$$

This new Hamiltonian reproduces all the magic numbers, i. e. 2,8,20,28,50,82,126 as can be seen on Figure.I.1.The two leftmost columns show the magic numbers and energies for a pure harmonic potential. The splitting of different values of the orbital angular momentum l can be arranged by modifying the central potential. Finally, the spin-orbit coupling splits the levels so that they depend on the relative orientation of the spin and orbital angular momentum. The number of nucleons per level $(2j + 1)$ and the resulting magic numbers are shown on the right [6].

Let's consider Figure.I.1:

- The spin-orbit coupling shifts the levels $j = l + 1/2$ downward while it shifts the levels $j = l - 1/2$ upward. In other words the parallel coupling of l and s is more attractive than the anti-parallel coupling [5].
- The nucleons are disposed on the levels from the bottom up and the degeneration of each level is given by $2j + 1$ [5].

- At high values of l the spin-orbit splitting becomes so strong intense that the harmonic oscillator shell structure is modified [6].
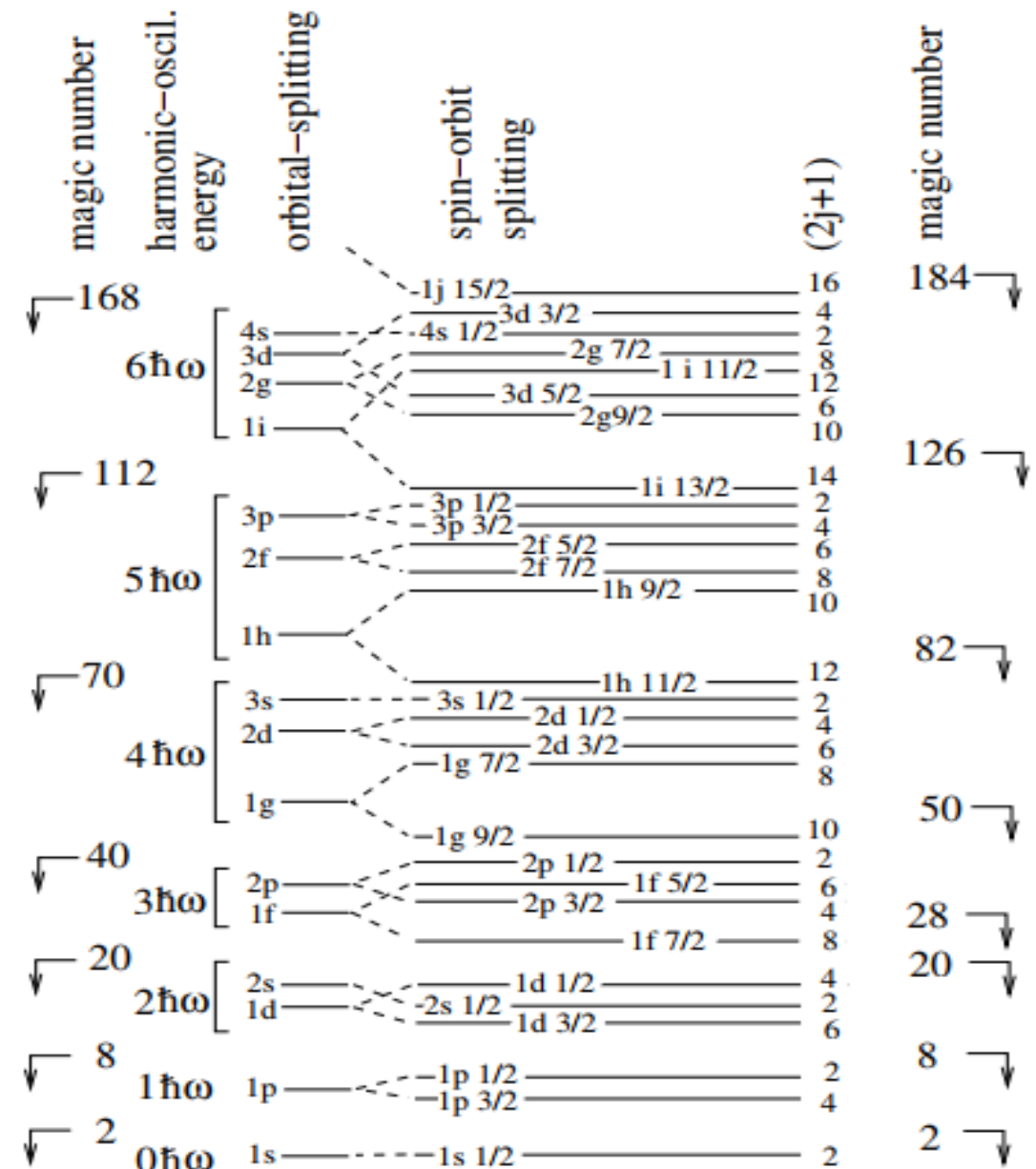
Figure.I.1: Nucleon orbitals in a model with a spin-orbit interaction [6].

I.4 Behind the mean field

The independent particles model is applicable only for spherical nuclei with single nucleon outside an inert core. The case of a nucleus with A interacting nucleons (Z protons and N neutrons) assumes that these nucleons interact in pairs with the two-body interaction V_{ij}. The Hamiltonian of this nucleus has the form [5]:

$$H = \left(\sum_{i=1}^{A}[t_i + U(i)] + \left[\sum_{i>j}^{A} V_{ij} - \sum_{i=1}^{A} U(i)\right]\right) = H_0 + H_r = \sum_{i=1}^{A} h_i + H_r \tag{21}$$

h_i: The individual Hamiltonian of a nucleon.

H_r**:** The residual two-body interaction, which is considered as a perturbation of the main

H_0 : Hamiltonian by an adequate choice.

I.5 Ingredientes of the shell model

Any shell model calculations require the following ingredients:

I.5.1 Choice of the valence space
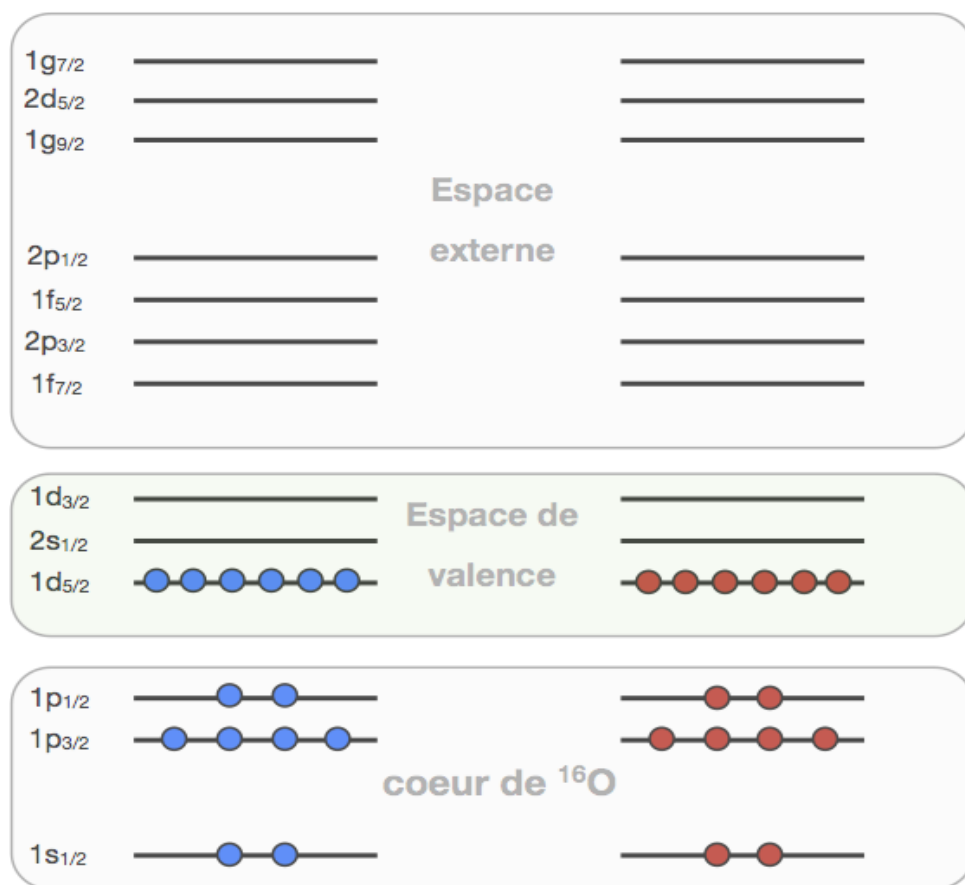
Figure I.2: Separation of the Hilbert space [7].

In the shell model approach, the Hilbert space Figure I.1 is divided into three parts as shown in Figure I.2 [7]:

- **An inert core,** which includes all the orbits always full, in general corresponds to a doubly magic nucleus. The core is composed of N_c neutrons and Z_c protons.
- **The valence space** corresponding to the set of orbits accessible to valence nucleons. These different orbits will be partially occupied by the valence nucleons [3]. When

studying a nucleus *X(Z,N)*, we must therefore consider $Z_v = Z - Z_c$ valence protons and $N_v = N - N_c$ valence neutrons [3].

- **External space**, with all the orbits, which will, bydefinition, always be empty in the calculations [3].

I.5.2 Effective interaction

Because of the strong short-range repulsion, the nucleon-nucleon interaction cannot be used directly for shell model calculations. These calculations are therefore based on the definition of an effective interaction, which is strongly linked to the valence space used. There are two types of effective interactions: realistic effective interactions and phenomenological effective interactions [3].

I.5.3 Shell model codes

Several codes have been developed in order to carry out shell model calculations. To our knowledge, the most used codes are: GLASGOW [8], ANTOINE [9], VECSSE [10], MSHELL [11], REDSTICK [12], RITSSCHIL [13], OXBASH [14], DUPSM [15], and NATHAN [9, 16]. We used in our calculations the code NATHAN.

I.6 Electromagnetic transitions in nuclear shell model

I.6.1 Electromagnetic transitions selection rules

During an electromagnetic transition in a nucleus from an initial state (i) (with energy E_i) to a final state (f) (with energy E_f), the nucleon emits or absorbs a gamma photon (with an energy E_γ). The principles of conservation of the energy and spin/parity make it possible to write [5]:

$$\begin{cases} E_\gamma = E_i - E_f \\ \pi_i \pi_\gamma \pi_f = +1 \end{cases} \tag{22}$$

The electromagnetic transition between these nuclear states can only take place if the emitted gamma photon carries a total angular momentum $\vec{L}$, with $\vec{J}_f = \vec{J}_i + \vec{L}$.

$$\left| \vec{J}_i - \vec{J}_f \right| \leq \Delta L \leq \vec{J}_i + \vec{J}_f \quad \text{and} \quad \Delta l > 0 \tag{23}$$
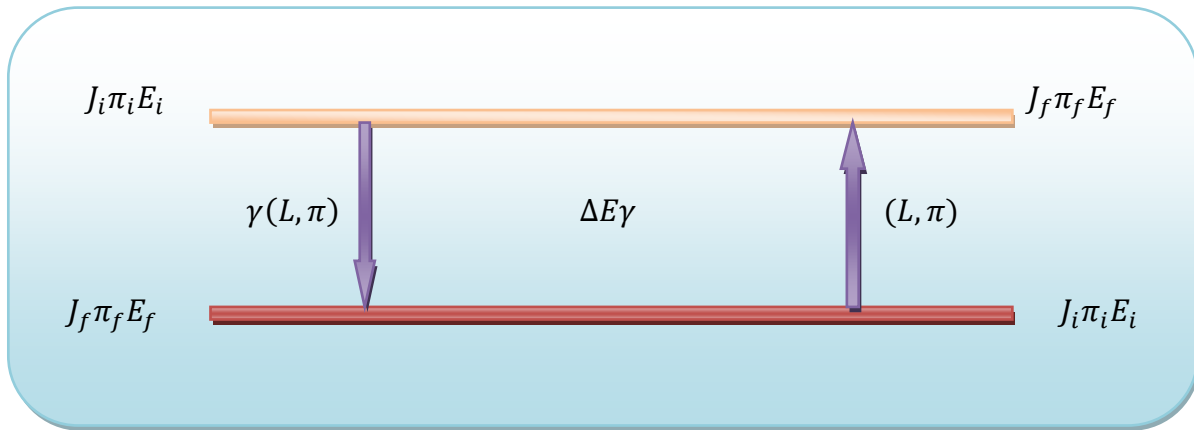
Figure I.3: Gamma emission and absorption in a nucleus.

As the intrinsic spin of the photon is equal to 1, the gamma transition with $L = 0$ is forbidden, and the gamma transition between states $\vec{J}_i = 0 \rightarrow \vec{J}_f = 0$ is thus forbidden. The angular momentum of the transition is called the multipolarity of the radiation. The character $2L$ –pole is dipole for $L = 1$, quadrupole for $L = 2$, octupole for $L=3$, ect [5].

$$\Delta \pi_\gamma = \begin{cases} \pi_\gamma = (-1)^L & if \ \sigma = EL \\ \pi_\gamma = (-1)^{L+1} & if \ \sigma = ML \end{cases} \qquad (24)$$

The multipole is of electric type EL when $\pi_\gamma = (-1)^L$ and magnetic ML when $\pi_\gamma = (-1)^{L+1}$. Therefore, γ transitions that connect states with the same parity will have even EL and odd ML, and those that connect states with different parities will have odd EL and even ML [5] (see Table I.1).

Table I.1: Selection rules for some electromagnetic transitions.

The Multipolarity	*Electric*		*Magnetic*	
	EL	*ΔJ Δπ*	*ML*	*ΔJ Δπ*
Dipolar	E_1	$1 -$	M_1	$1 +$
Quadrupole	E_2	$2 +$	M_2	$2 -$
Octupole	E_3	$3 -$	M_3	$3 +$

I.6.2 Probabilities of electromagnetic transitions

The transition probability of (electric or magnetic) transition of multipolarity L is given by [5]:

$$B(\sigma L; J_i \rightarrow J_f) = \frac{1}{2J_i+1} \left| \langle \psi_f \| \mathcal{M}(\sigma \mathrm{L}) \| \psi_i \rangle \right|^2 \tag{25}$$

With the total angular momentum J_i and J_f of the initial state $|\psi_i\rangle$ and the final state $|\psi_f\rangle$ respectively, $\langle \psi_f \| \mathcal{M}(\sigma \mathrm{L}) \| \psi_i \rangle$ is the reduced transition matrix element with the electromagnetic multipole operator $\mathcal{M}(\sigma \mathrm{L})$, which can have either an electric ($\sigma L = EL$) or a magnetic ($\sigma L = ML$) character. The transition matrix element $\mathcal{M}(\sigma \mathrm{L})$ of an electromagnetic decay of an excited state is the same transition matrix element as of the excitation process with the same σL character. Therefore thetransition strength of the excitation and de-excitation between two states with J_i and J_f is connected by [5]:

$$B(\sigma \mathrm{L}; J_i \rightarrow J_f) = \frac{2J_f+1}{2J_i+1} B(\sigma \mathrm{L}: J_f \rightarrow J_i) \tag{26}$$

The value of $B(EL)$ is usually expressed in terms of $e^2 b^L = 10^4 \, e^2 fm^{2L}$, whereas $B(ML)$ is given in $\mu_N^2 b^{L-1} = 10^4 \mu_N^2 fm^{2(L-1)}$, with μ_N the nuclear magneton. In a single-particle picture, where only one single nucleon contributes to the electromagnetic transition, the so-called "Weisskopf unit" (W.u.) can be defined [5]:

$$B(EL)_W = \frac{1}{4\pi} \left(\frac{3}{L+3} \right)^2 (1.2A^{1/3})^{2L} \tag{27}$$

$$B(ML)_W = \frac{10}{\pi} \left(\frac{3}{L+2} \right)^2 (1.2A^{1/3})^{2L-2} \tag{28}$$

In many experiments the lifetime τ of an excited state is measured to determine the transition probability. The probability for the emission of a γ ray of multipolarity L from an excited state J_i in to a lower-lying state J_f is connected to the $B(\sigma L)$ value and is expressed by [5]:

$$\mathrm{T}(\sigma \mathrm{L}; J_i \rightarrow J_f) = \frac{8\pi(L+1)}{\hbar L[(2L+1)!!]^2} \left(\frac{E_\gamma}{\hbar c} \right)^{2L+1} B(\sigma \mathrm{L}; J_i \rightarrow J_f) \tag{29}$$

The lifetime of a state J_i, which can decay into several final states J_f by emission of L-pole radiation, is given by [5]:

$$\tau(J_i) = \left(\sum_{J_f} \sum_\lambda \mathrm{T}(\sigma \mathrm{L}; J_i \rightarrow J_f)[1 + \alpha(L)] \right)^{-1} \tag{30}$$

Including the usual L-pole conversion coefficient $\alpha(L)$.

The nucleus is composed of an inert core plus a valence particle. The transitions take place between states $J_i = \text{L} \pm 1/2$ and $J_f = 1/2$ of this core. The radial parts of the initial and final state wave functions are both constant inside the nucleus of radius R and zero outside [5].

$$B(EL) = \frac{9}{4\pi(L+3)^2} e^2 R^{2L} \frac{\Gamma_\gamma}{\Gamma_w} (e^2 fm^{2L}) \tag{31}$$

$$B(ML) = \frac{90}{\pi(L+3)^2} \mu_N^2 R^{2L-2} \frac{\Gamma_\gamma}{\Gamma_w} (\mu_N^2 fm^{2L-2}) \tag{32}$$

With $R = 1.2A^{\frac{1}{3}}(fm)$, e is the electric charge and $\mu_N = \frac{e\hbar}{2mc}$ is the nuclear magneton. Γ_γ and Γ_w are the transition width and the Weisskopf estimate (in eV) (see Table I.2), respectively. We define "the strength of a transition" in Weisskopf units (u.W.) by the formula [5]:

$$S = \frac{\Gamma_\gamma}{\Gamma_w} \tag{33}$$

Table I.2: Single-particle width (Weisskopf estimate) Γ_w (W. u.) in MeV [5].

Electric	*Magnetic*
$\Gamma_w(E1) = 68\, A^{2/3} E_\gamma^3$	$\Gamma_w(M1) = 21\, E_\gamma^3$
$\Gamma_w(E2) = 4.9 \times 10^{-5} A^{4/3} E_\gamma^5$	$\Gamma_w(M2) = 1.5 \times 10^{-5} A^{2/3} E_\gamma^5$
$\Gamma_w(E3) = 2.3 \times 10^{-11} A^2 E_\gamma^7$	$\Gamma_w(M3) = 6.8 \times 10^{-12} A^{4/3} E_\gamma^7$
$\Gamma_w(E4) = 6.8 \times 10^{-18} A^{8/3} E_\gamma^9$	$\Gamma_w(M4) = 2.1 \times 10^{-18} A^2 E_\gamma^9$
$\Gamma_w(E5) = 1.6 \times 10^{-24} A^{10/3} E_\gamma^{\square 1}$	$\Gamma_w(M5) = 4.9 \times 10^{-25} A^{8/3} E_\gamma^{11}$

I.6.3 Operators

❖ Electric operator

The electric operator is given by the following formula [5]:

$$\mathcal{M}_{LM} = \sum_{i=1}^{A} e(k)\, r^L(k) Y_{LM}(r(k)) \tag{34}$$

Where $e(k)$ denotes the free electric charge of a nucleon k, that equal:

$$\begin{cases} e(k) = 0 \Rightarrow for\ neutrons \\ e(k) = e \Rightarrow for\ protons \end{cases}$$

❖ Magnetic operator

The magnetic operator is given by the following formula [5]:

$$\mathcal{M}_{LM} = \sum_{i=1}^{A} \mu_N \left[g^s(k)\vec{s}(k) + \frac{2g^l(k)}{L+1}\vec{l}(k) \right].\nabla(k)r^l(k)Y_{LM}(r(k)) \tag{35}$$

μ_N Is the nuclear magneton given by $\mu_N = \frac{e\hbar}{2mc}$.

$g^l(k)$ and $g^s(k)$ denote the orbital and spin gyromagnetic factors, respectively. In TableI.3 are presented the free orbital and spin$g$ factors values [5].

TableI.3: Free orbital and spin g factors values [5].

$g(k)$	Protons	Neutrons
$g^s(k)$	5.586	-3.826
$g^l(k)$	1	0

❖ *Notes*

The reduced probability of a transition B(E2) allows figuring out if the transition is due to an individual or collective contribution of nucleons in the nucleus. Indeed, the B(E2) is rather weak for a spherical nucleus and higher for a collective or deformed nucleus.

If the initial state decreases to different final states, then the total transition width Γ_T is the sum of the partial widths [5]:

$$\Gamma_T = \sum_k \Gamma_{\gamma k} \tag{36}$$

The half-life is given according to the meanlife-time by [5]:

$$T_{1/2} = \tau.ln2 \tag{37}$$

In this chapter we started by stating the magic numbers and the shell structure from the nuclear shell model, beyond the mean field and the shell model ingredients. The second part of this chapter introduces essential tools, which are the electromagnetic transitions.

In the next chapter we deal with the sd-shell nuclei, an area of our current work.

Chapter II

Chapter II

Description of sd-shell nuclei and the PSDPF interaction

In recent years, researchers have paid attention to the properties of nuclei that belong to the sd-shell region, and they have been the subjects of many experimental studies.

In this chapter we introduce the properties of sd-shell nuclei. Then we present the PSDPF interaction that has been developed and succeeded in characterizing the properties of nuclei throughout the sd-shell.

II.1 sd-shell nuclei

The region of sd-shell nuclei is comprised between the magic doubling nuclei ^{16}O and ^{46}Ca. These nuclei contain a number of protons and neutrons between 8 and 20 includes. There are 146 experimentally known nuclei of which 26 are stable (Figure II.1). These nuclei are characterized, at low excitation energy, by the coexistence of normal positive"+" parity states and intruded negative "−" parity states [3].

In our thesis, we are interested in studying the structure of "^{26}**Mg**", situated in the middle of the sd-shell.
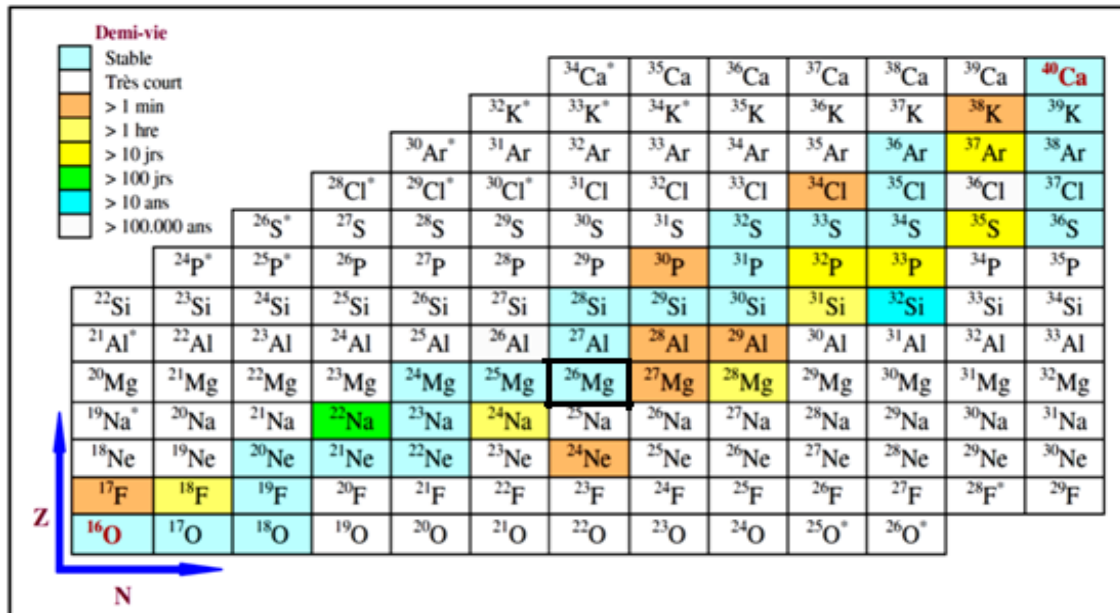
Figure II.1: Chart of the sd-shell nuclei [17].

II.2 States in sd-shell nuclei

II.2.1 Normal states

The normal positive parity states in the sd-shell nuclei result from the distribution of the active nucleons, whose number is (*A-16*), within the sd valence space (0ℏω space). Thi**s** and **p** shells are filled and inactive to form an inert "**¹⁶O**" core. This implies the configuration 0 particles-0 holes (0p-0h), hence the name of states 0ℏω. The interactions describing are usd [18], usd A or B [19].

II.2.2 Intruder States

The sd-shell nuclei may have two types of intruder states corresponding to the promotion of one nucleon or more across the p-sd or sd-pf shells. We explain their carachterestics in the following sections.

II.2.2.1 Positive parity states

In an sd nucleus, we can find positive parity intruder states for which the configuration is outof the sd valence space and possess a (2p−2h) configuration for the 2ℏω states or (4p−4h) forthe 4ℏω states, the corresponding nucleus is generally deformed. These effects were observed in the doubly magic nuclei,¹⁶O, and ⁴⁰Ca [3].

II.2.2.2 Negative parity states

The intruder states with negative parity result from the promotion of one nucleon from p to sd or from sd to pf shells, these states have a (1p−1h) configuration and are also called 1ℏω states. The interaction describing the 1ℏω states is the PSDPF interaction [3,20]. In this case,the model space is extended to the full p-ds-pf space and the inert core is ⁴He. These states appear at low excitation energies [17].

The sd nuclei that possess observed 1ℏω intruder states are shown in Figure II.2.

II.3 The PSDPF interaction

In order to describe simultaneously both negative and positive parity states in sd-shell nuclei, and the transitions between these different states, we use the (0+1)ℏω PSDPF interaction developed in Strasbourg by M. Bouhelal and al. [3,20]. In this case, the core used is restricted to the ⁴He doubly magic nucleus and the valence space includes the p,sd and pf shells, containing the 9 sub-shells: $1p_{3/2}$, $1p_{1/2}$, $1d_{5/2}$, $2s_{1/2}$, $1d_{3/2}$, $1f_{7/2}$, $2p_{3/2}$, $1f_{5/2}$, $2p_{1/2}$.
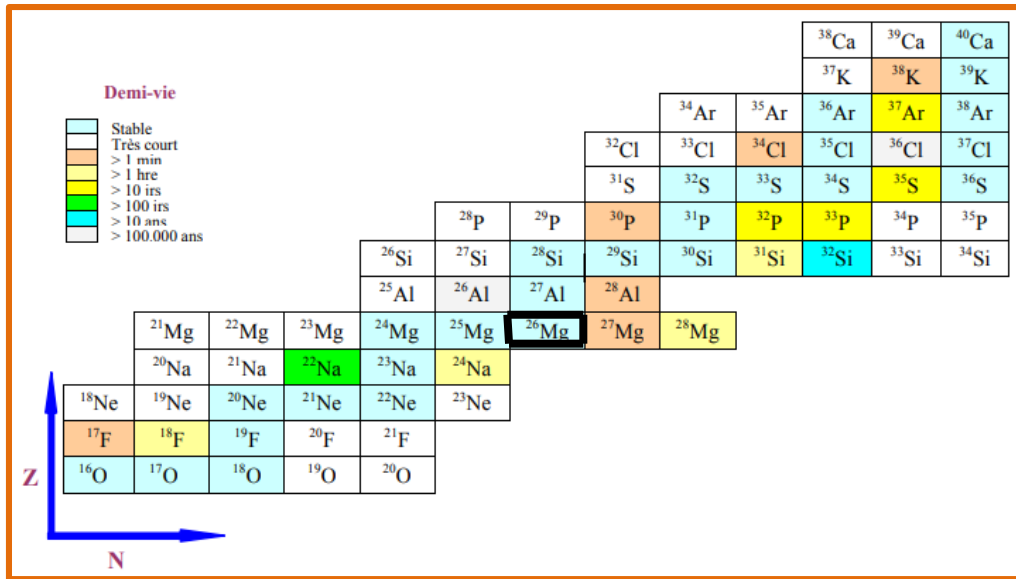
Figure II.2: Chart of sd nuclei with known negative parity intruder states [17].

II.4 Shell model ingredients for sd-shell nuclei

- Valence space: the full $p - sd - pf$ space.
- Compatible interaction with this space: **PSDPF** interaction.
- Code of calculation: the shell model code **NATHAN** [9, 16].

II.5 Description of positive and negative parity states in sd nuclei

The sd-shell nucleus that interested usin our thesis is the ^{26}Mg, with 12 protons and 14 neutrons. In this nucleus, the ground state is 0^+ that corresponds to the fulfilling $1d_{5/2}$ sub-shell, i.e. containing 12 nucleons(6 protons and 6 neutrons). Figure II-3 represents an example of the first excited positive - and negative – parity states, 2^+ and 3^- , respectively, and the ground 0^+ state in ^{26}Mg.

- The first negative parity excited state 3^- in (b), results from the jump of a proton from the $1p_{1/2}$ sub-shell towards the $1d_{5/2}$ sub-shell with a probability of 08%.
- The first positive parity excited state 2^+ shown in part (c), results from the occupation of the $1d_{5/2}$ from the valence protons and neutrons with a probability of 19%.
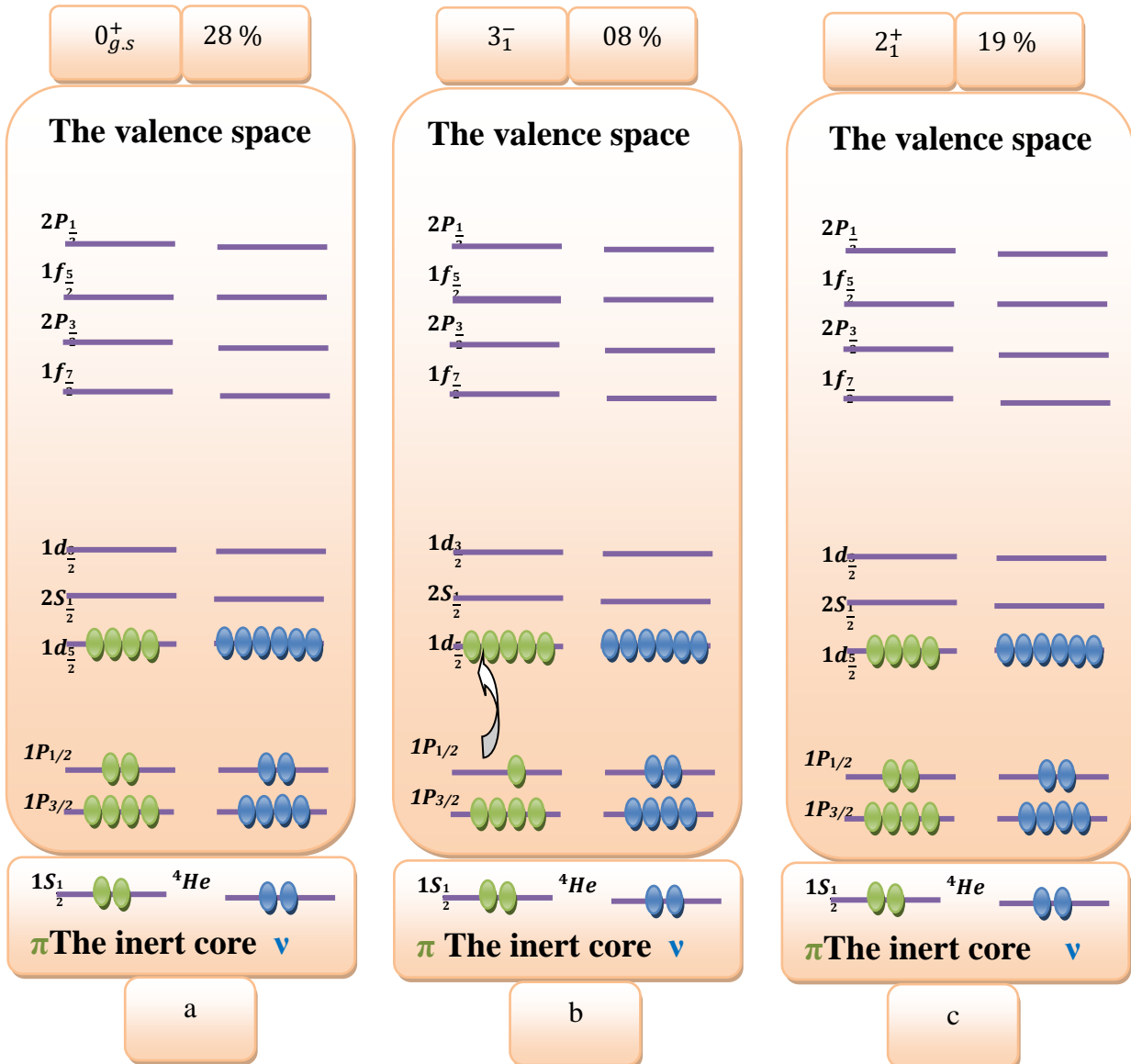
Figure II.3: Shematic distribution of (a) the ground state (b) the first $1\hbar\omega$ excited state in ^{26}Mg and (c) the first $0\hbar\omega$ excited state.

II.6 Electromagnetic Transitions in the sd Nuclei

The PSDPF interaction reproduced the energy spectra of several sd nuclei and some isotopic chains [21-58] and provided great success in describing the 0 and 1ħω states of nuclei across the sd-shell. The electromagnetic transitions are a useful test of the wave functions for each evolving interaction. The electromagnetic operators need the following parameters: effective charges and gyromagnetic factors. Transitions between positive parity states E2 and M1 have been studied using USDA/B interactions [60].

M. LABIDI has studied the E3 transitions by adjusting its effective charges to available experimental values [28, 59]. The obtained parameters for the three E2, M1 [60] and E3[28, 59] transitions are presented on Table II.1.

Table II .1: Adjusted parameters for the transitions E2, M1 and E3.

W. A. Richter and B. A. Brown [60]		M. Labidi[28, 59]
Effective charges (E2)	**Gyromagnetic factors (M1)**	**Effective charges (E3)**
$e_p = 1.36$	$g^l{}_p = 1.159$	$e_p = 1.36$
	$g^s{}_p = 5.150$	
$e_n = 0.45$	$g^l{}_n = -0.090$	$e_n = 0.48$
	$g^s{}_n = -3.550$	

In this chapter, we have identified the sd-shell nuclei region, described some of its properties. An illustration of a specific probability distribution for the first two excited states with positive - and negative - parity as well as the ground state was shown. The last chapter is dedicated to the study of the spectroscopic properties of $^{26}M_g$.

Chapter III

Chapter III

Spectroscopic properties of ^{26}Mg

In the first and second chapters, we have looked over the concepts of the nuclear shell model, the properties of the sd nuclei, and the PSDPF interaction. In this chapter, we will calculate the spectroscopic properties of ^{26}**Mg** using the Nathan code and the PSDPF interaction and compare the results with available experimental data. The aim of our work here is to identify the ambiguous states.

III.1 Experimental versus calculated spectroscopic properties of ^{26}Mg

We used the computational code Nathan and the (0+1)ℏω **PSDPF** interaction to calculate some spectroscopic properties of ^{26}**Mg**.We discuss in the following session the comparison experimental versus theory separately for the energy spectrum and strengths of the transitions in Weisskopf units (u.W.).

III.1.1 Energy spectrum

^{26}**Mg** is a neutron-rich nucleus that has Z < N, its energy spectrum is experimentally well studied up to around 5.6 MeV. We used the analogous T = 1 states in ^{26}**Si** and ^{26}**Al**, which enables us confirm the uncertain states to assign all the ambiguous states in ^{26}**Mg** with their appropriate spin/parity, **J$^\pi$**, values. We present on Table III.1 the comparison experimental versus calculated excitation energies on columns 2 and 4, and the **J$^\pi$** values on columns 1 and 3, respectively. In the last column we show difference in energy, ΔE = E$_{Th}$ - E$_{exp}$ .The energy differences give us information about our results as follows:

- States with ΔE> 400 keV (shown in red on Table III.1), have a collective contribution with more than 0p-0h or 1p-1h configurations for + or – states, respectively, and those with ΔE≥ 1 MeV are pure collective states.
- ΔE< −400 keV (shown in blue) are not well reproduced using PSDPF.

Table III. 1: Experimental versus calculated energy spectra of **^{26}Mg**.

E_{Mg}		E_{Th}		$\Delta E = E_{Th} - E_{Ex}$
$J\pi$	E	J_i^π	E	
0+	0	0_1^+	0	0
2+	1,809	2_1^+	1,878	0,069
2+	2,938	2_2^+	3,042	0,104
0+	3,589	0_2^+	3,829	0,24
3+	3,942	3_1^+	3,99	0,048
4+	4,319	4_1^+	4,397	0,078
2+	4,333	2_3^+	4,59	0,257
3+	4,35	3_2^+	4,389	0,039
2+	4,835	2_4^+	4,944	0,109
4+	4,901	4_2^+	5,013	0,112
0+	4,972	0_3^+	4,909	-0,063
	5,181	2_5^+	5,5	0,319
2+	5,292	2_6^+	6,668	1,376
4+	5,476	4_3^+	5,553	0,077
(1+)	5,691	1_1^+	5,693	0,002
(1+,2+)	5,711	1_1^-	6,663	0,952
4+	5,716	4_4^+	5,925	0,209
3+	6,125	3_3^+	6,283	0,158
0+	6,256	0_4^+	6,278	0,022
(4+)	6,623	4_5^+	6,815	0,192
	6,634	1_2^+	6,668	0,034
2+	6,745	2_7^+	6,936	0,191
3-	6,876	3_1^-	6,716	-0,16
(5+)	6,978	5_1^+	7,086	0,108
1-	7,062	1_2^-	7,49	0,428
2+	7,1	2_8^+	7,214	0,114
(0 ,1)+	7,2	0_5^+	8,07	0,87
3+	7,246	3_4^+	7,341	0,095
	7,261	2_1^-	6,736	-0,525
(4-)	7,283	4_1^-	7,898	0,615
3-	7,349	3_2^-	7,495	0,146
2+	7,371	2_9^+	7,575	0,204
(5+)	7,396	5_2^+	7,447	0,051
(0,1)+	7,428	1_3^+	7,93	0,502
(2-)	7,542	2_2^-	7,697	0,155
(4+)	7,677	4_6^+	7,53	-0,147
1(-)	7,697	1_3^-	7,728	0,031
3+	7,726	3_5^+	7,7	-0,026
(4+)	7,774	4_7^+	7,883	0,109
(2 ,3)+	7,818	3_6^+	8,301	0,483
3-	7,824	3_3^-	7,935	0,111
2+	7,84	2_{10}^+	8,379	0,539
	7,851	2_3^-	7,951	0,1
5-	7,95	5_1^-	8,318	0,368
	8,034	2_{11}^+	8,993	0,959
2(+)	8,052	2_4^-	8,145	0,093

3-	8,185	3_4^-	8,195	0,01
(6+)	8,201	6_1^+	8,252	0,051
1-	8,227	1_4^-	8,041	-0,186
(3+)	8,251	3_5^-	8,554	0,303
	8,399	4_2^-	8,396	-0,003
(3+)	8,459	3_7^+	8,536	0,077
	8,464	4_8^+	8,682	0,218
(6+)	8,472	6_2^+	8,56	0,088
1-	8,504	1_5^-	8,724	0,22
(2+)	8,532	1_4^+	8,443	-0,089
	8,576	0_6^+	8,831	0,255
5-	8,625	5_2^-	9,063	0,438
(3,5)	8,67	5_3^+	8,49	-0,18
(2 To 4)+	8,706	2_5^-	8,73	0,024
	8,706	4_9^+	8,757	0,051
2+	8,864	2_{12}^+	9,359	0,495
(2+)	8,904	2_6^-	8,824	-0,08
	8,93	4_{10}^+	9,219	0,289
1-	8,959	1_6^-	8,776	-0,183
	9,02	4_3^-	8,773	-0,247
3(+)	9,043	3_6^-	8,777	-0,266
5+	9,064	5_4^+	9,182	0,118
6+	9,111	6_3^+	9,17	0,059
1	9,14	1_7^-	9	-0,14
(6-)	9,169	6_1^-	9,426	0,257
	9,206	4_4^-	9,548	0,342
1(+)	9,239	1_8^-	9,274	0,035
(4+)	9,261	4_{11}^+	9,34	0,079
(2+)	9,281	2_{13}^+	9,489	0,208
	9,291	3_7^-	9,119	-0,172
	9,304	2_{14}^+	9,556	0,252
	9,316	2_{15}^+	9,89	0,574
(2+ To 4+)	9,326	4_{12}^+	9,409	0,083
4+	9,371	4_{13}^+	9,855	0,484
6+	9,383	6_4^+	9,69	0,307
3+	9,428	3_8^+	9,199	-0,229
(1 To 5)+	9,471	3_9^+	9,405	-0,066
	9,471	1_5^+	9,416	-0,055
5+	9,54	5_5^+	9,575	0,035
1+	9,564	1_6^+	9,452	-0,112
(2- To 4)	9,574	3_8^-	9,478	-0,096
4+	9,579	4_{14}^+	10,175	0,596
	9,59	2_{16}^+	10,269	0,679
	9,857	2_{17}^+	10,491	0,901
(0 To 5)+	9,681	3_{10}^+	9,689	0,008

1(-)	9,771	5_3^-	9,649	-0,122
	9,771	1_9^-	9,915	0,144
	9,771	1_8^+	10,138	0,367
1+	9,779	1_7^+	9,649	-0,13
	9,779	1_9^+	10,527	0,748
	9,814	5_6^+	9,694	-0,12
(5,7)+	9,83	7_1^+	9,788	-0,042
	9,883	5_7^+	10,249	0,366
3+	9,9	3_{11}^+	10,093	0,193
	9,927	4_5^-	10,039	0,112
	9,982	3_{12}^+	10,531	0,549
(6+)	9,989	6_5^+	10,037	0,048
5-	10,04	5_4^-	9,858	-0,182
	10,069	5_5^-	10,301	0,232
1-	10,103	1_{10}^-	10,022	-0,081
0+	10,159	0_7^+	10,161	0,002
		0_1^-	8,004	

The spectrum of ^{26}**Mg** contains the **107**, among them **35** have negative eparity, and **72** have positive parity .All the observed states have their theoretical counter parts. Based on this comparison, the ΔE differences for each **J^π** value concerning + and – states are shown on Figures III.1 and III.2, respectively. All the + states were either quite well described using PSDPF or have a collective character. Concerning the – states, most of the observed states are are in good agreement using PSDPF, except for the proposed 2_1^-. Few – states have collective configuration. All the uncertain states having **J^π** in parenthesis were confirmed following this study. In addition, we were able to attribute spin/parity values for all states with unknown **J^π**.

In order to illustrate well the collective states for each **J$^+$** and **J$^-$** value in the studied nucleus, we present on Figures III.3 and III.4, respectively, the comparison experimental versus calculated of their excitation energies. We can see that the variation of the excitation energies for all the **J^π** values are remarkably well described by PSDPF and the both experimental and theoretical values have the same shape.
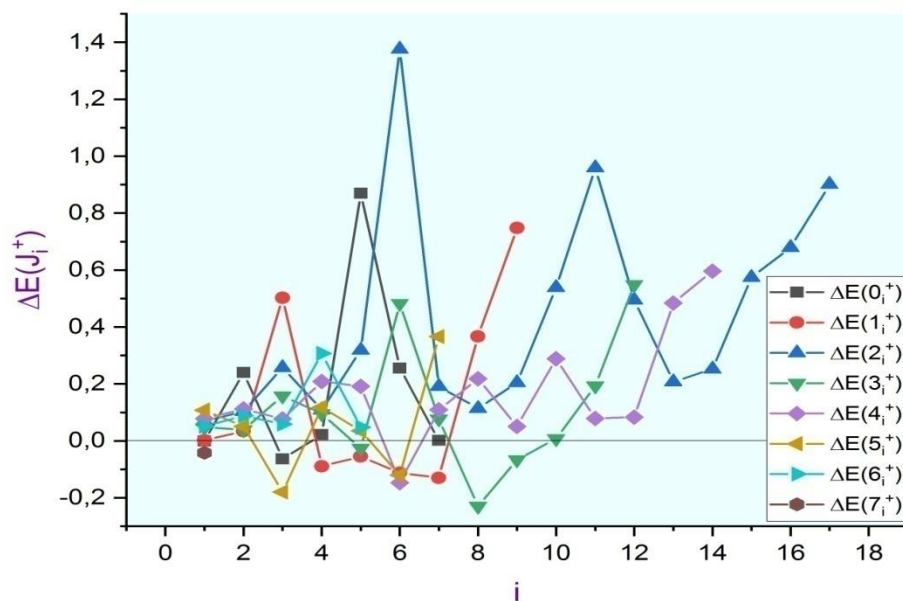
Figure III. 1: Energy difference, **ΔE**, for the **J**+ states in **^{26}Mg**.
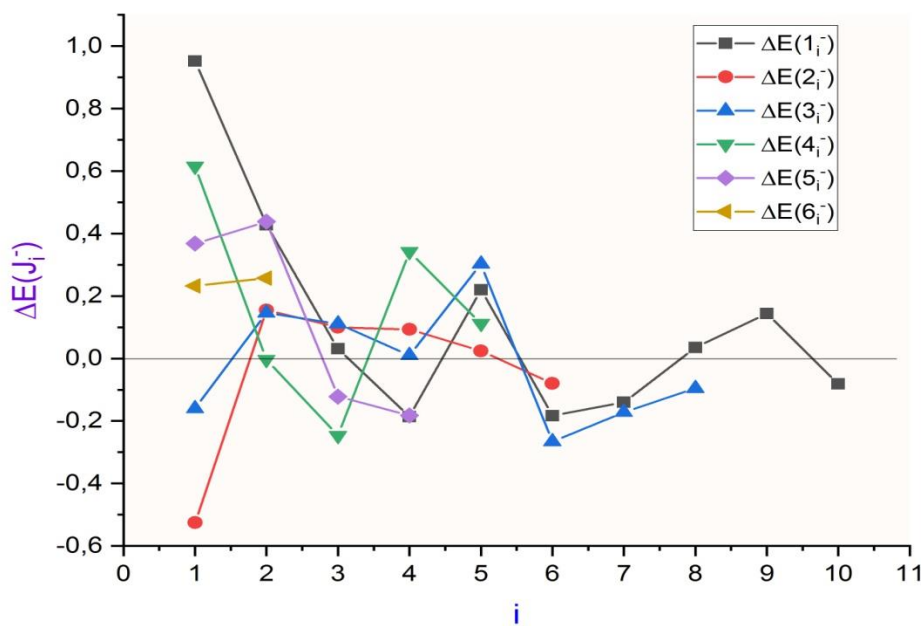

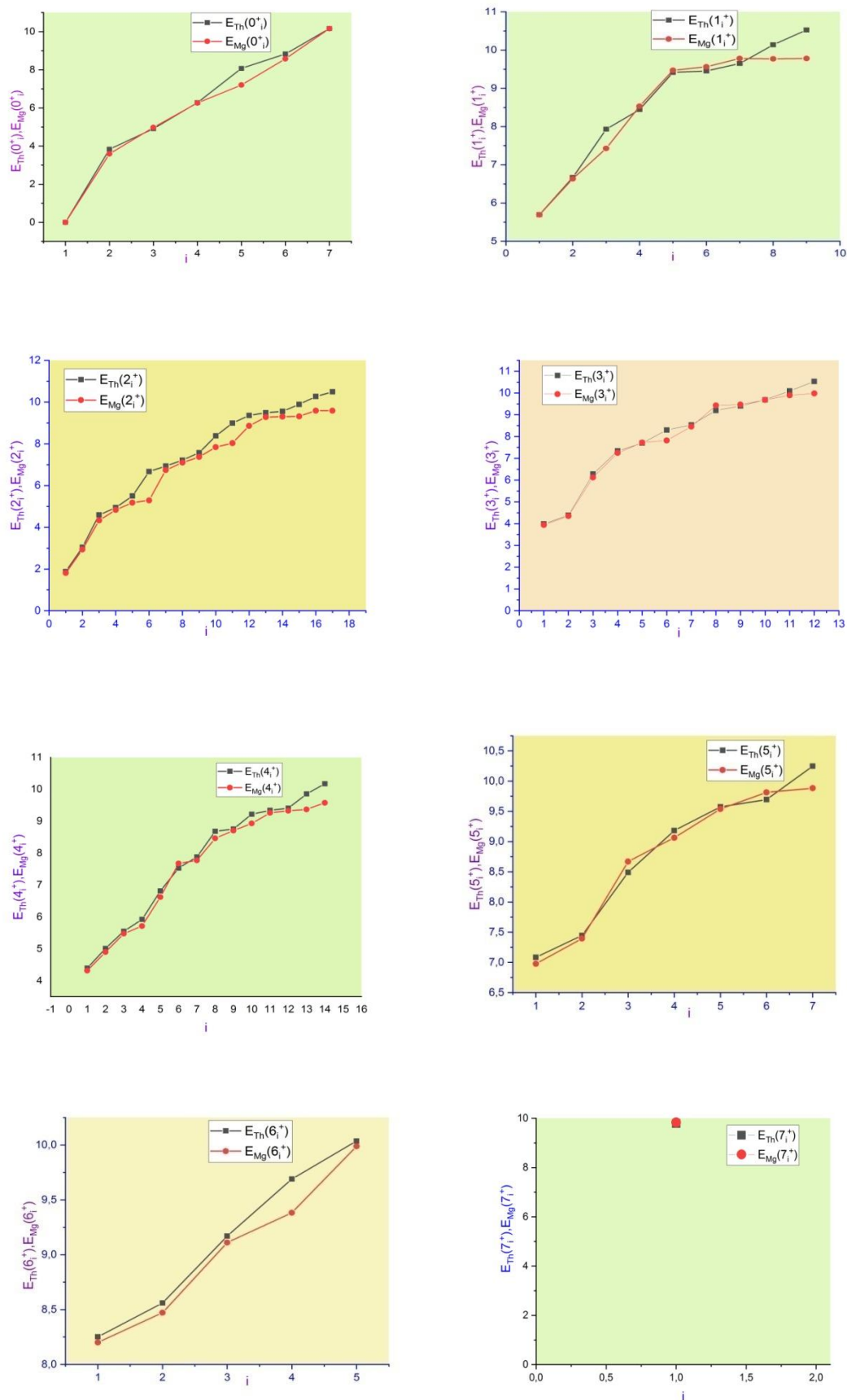**Figure III. 2:** Energy difference, **ΔE**, for the **J**- states in **^{26}Mg**.

Figure III. 3: Experimental versus calculated excitation energies for each **J⁺** in **²⁶Mg**.
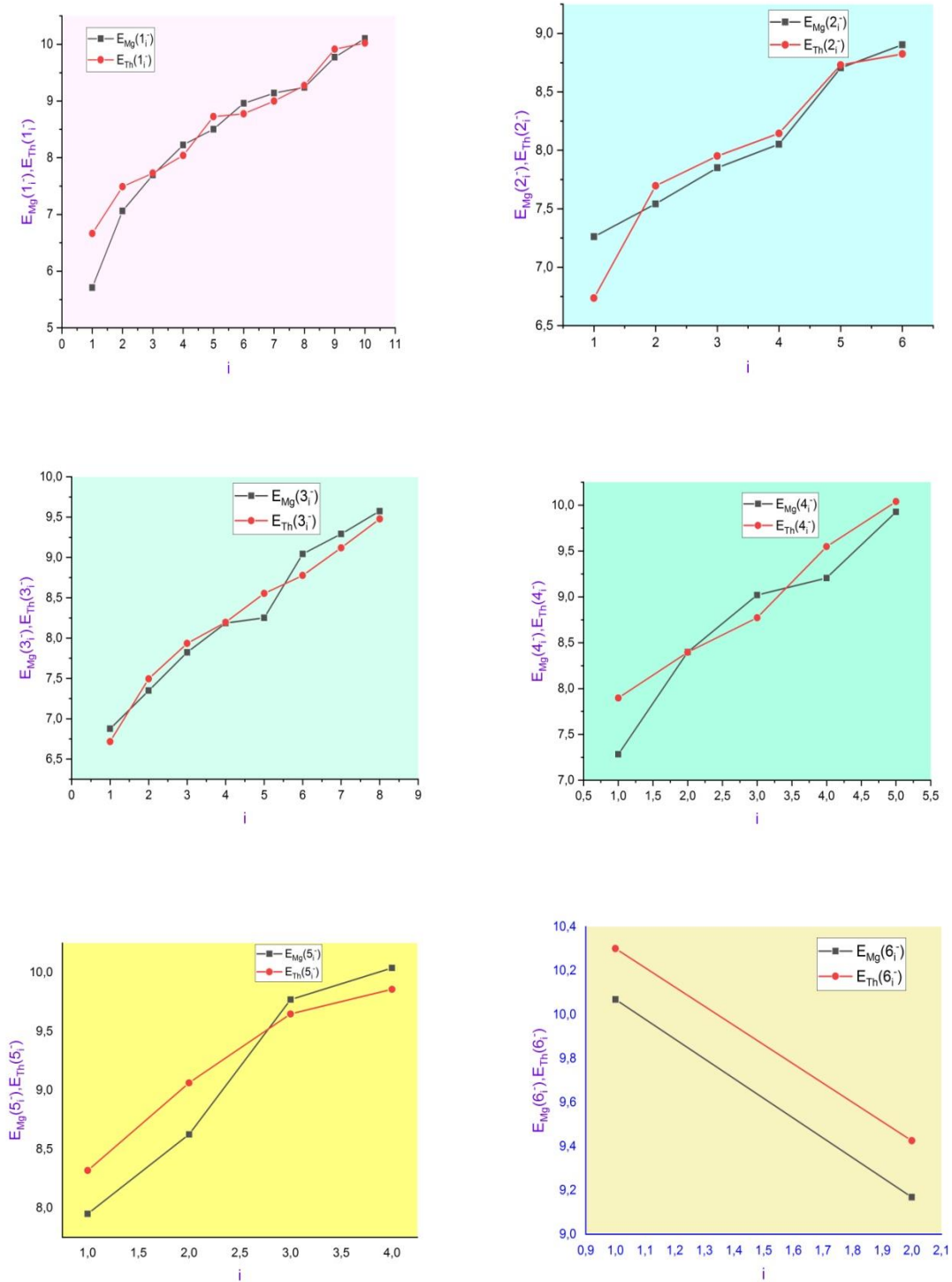
Figure III.4: Experimental versus calculated excitation energies for each **J⁻** in **²⁶Mg**.

III.1.2 Strengths of the transitions

After the remarkable success of the PSDPF interaction in describing the energy spectrum of the **26Mg** nucleus, we calculated the strengths of the transitions in Weisskopf units (u.W.) defined in the previous chapter in eq. 33. In our calculation we used the effective charges and gyromagnetic factors given on Table II.1, for Electric EL transitions and Magnetic ML transitions, respectively. Note that the same gyromagnetic factors have been used for both M1 and M2 transitions. The calculated strengths of the transitions in Weisskopf units (u.W.) are compared with the experimental ones on Tables III. 2. On this Table, we show the **Jπ** of the initial and final states in columns 1 and 3 and the nature of the transition **(σL)** relating these states is presented in column 2. In the 2 last columns, we compare calculated and experimental (with the errors) strengths of the transitions **S**.

Table III.2: Comparison experimental versus calculated strengths of the transitions in Weisskopf units (u.W.) of **26Mg**

J_i^π (ini)	σL	J_i^π (fin)	S_{Th} [u.W]	S_{Ex} [u.W]
2_1^+	E_2	0_2^+	0,01	1.07 $\pm$0.08
2_1^+	E_2	0_3^+	0,002	0.06 $\pm$0.04
2_2^+	E_2	0_3^+	0,34	7.4 $\pm$1.3
2_1^+	E_2	0_4^+	0,05	1.2 $\pm$0.8
2_1^+	E_2	0_1^+	15.01	13.4 $\pm$0.6
2_2^+	E_2	0_1^+	0,91	0.39 $\pm$0,4
	E_2	2_1^+	8,2	6.1$\pm$ 2,1.
	M_1		0,09	0.096$\pm$ 0,006
2_3^+	E_2	0_1^+	0,02	0.24$\pm$ 0.05
2_4^+	E_2	0_1^+	0,16	0.15 $\pm$0.04
	M_1	2_2^+	0,001	0.096 $\pm$0.021
2_6^+	E_2	0_1^+	0,03	>0.10
	M_1	3_1^+	0,00026	>0.026
3_1^+	E_2	2_2^+	0,003	0.23 +37−22
	M_1		0,0055	0.0162 $\pm$24
	M_1	2_1^+	0,00089	0.00104 $\pm$16
3_2^+	E_2	2_1^+	1,45	0.06$\pm$ 0.05
	M_1		0,0124	0.0066 $\pm$18
	E_2	2_2^+	24	9 $\pm$4
	M_1		0,03	0.033 $\pm$9

3_3^+	M_1	3_2^+	0,41	0.20 $\pm$0.90
4_1^+	E_2	2_1^+	4,5	4.5 $\pm$0.3
4_2^+	E_2	2_1^+	13	14 $\pm$0.3
		2_2^+	3	2.5 $\pm$0.6
4_3^+	E_2	2_1^+	1,3	1.1 $\pm$0.4
	E_2	3_1^+	17,1	12 $\pm$5
	M_1		0.083	0.071 $\pm$0.022
	E_2	4_1^+	2,16	12 +19−11
	M_1		0,28	0.34 $\pm$0.10
4_4^+	E_2	2_1^+	1,4	3.1$\pm$ 1.4
	E_2	3_1^+	1,11	0.036 $\pm$0.010
	M_1		0,002	0.4$\pm$ 0.2
	E_2	3_2^+	7,591	0.017$\pm$ 5
	M_1		0,03	1.7$\pm$ 0.5
4_5^+	E_2	2_3^+	11,25	12 $\pm$4
	E_2	4_2^+	0,69	0.09$\pm$ 4
	M_1		0,067	12 +52−8
	M_1	4_3^+	0,0214	0.063$\pm$ 0.018
5_1^+	E_2	3_1^+	3,67	4.8 $\pm$1.9
		3_2^+	1,99	1.5$\pm$ 1.2
	E_2	4_1^+	4,412	0.012$\pm$ 0.005
	M_1		0,01	3.2$\pm$ 1.4
	E_2	4_2^+	4,7	13$\pm$ 9
	M_1		0,01	0.010$\pm$ 0.007
	E_2	4_3^+	10	24 $\pm$15
	M_1		0,1	0.22$\pm$ 0.09
5_2^+	E_2	4_4^+	3,4	>4.6
	M_1		0,17	>0.16
6_3^+	E_2	4_1^+	1,17	>0.80
		4_2^+	1,02	>1.4
		4_3^+	11,1	>8.8
		4_4^+	0,3	>9.4
	M_1	5_2^+	0,03	>0.032
7_1^+	E_2	6_1^+	0,13	<18
	M_1		0,06	>0.084
1_1^-	E_1	0_2^+	0,00081	>0.00089
		2_1^+	0,00142	>0.00015
1_8^-	E_1	0_1^+	0,006	0,072$\pm$0.00 9
3_1^-	E_1	3_1^+	0,00032	0,000011 $\pm$0,000005
4_1^-	E_1	3_1^+	0,00022	0,00043 $\pm$15
	E_1	4_1^+	0,0004	40 +60−30
	M_2		0,00044	0,00031$\pm$ 15
5_1^-	E_1	4_1^+	0,0018501	0,0008$\pm$ 4
	M_1		0,03	5 +8−4
	E_1	4_4^+	0,31	50 +80−40

	M_1		0,02	$0,0015 \pm 0.0007$
	E_1	4_1^+	0,0018	0.000051 ± 0.000016
5_2^-	E_1	4_5^+	0,0011	$2,9 \pm 2.1$
	M_2		0,0004	$0,0028 \pm 0.0006$
	E_1	5_1^+	0,000000307	$0,00034 \pm 0.00013$
	E_2	4_1^-	10,5	26 ± 10
6_1^-	E_1	5_2^+	0,00128	$8 + 12 - 7$
	M_2		0.01163	$0,0011 \pm 0.0004$
	E_2	5_1^-	20,9	18 ± 17
	M_1		0,078	$0,25 \pm 0.08$

This table represents **29** initial states whose strengths were measured. Most of these states have more than one electromagnetic transition type **(σL)**. For example, the $J_i^\pi(ini) = 5_1^+$ state has 5 final equivalence states with pure **E₂** transition to the final states $J_i^\pi(fin) = 3_1^+, 3_2^+$; and a substitution **M1+E2** transitions to the $J_i^\pi(fin) = 4_1^+, 4_2^+, 4_3^+$.

Almost all the measured strengths are quite well reproduced using the PSDPF interaction within the bar errors.

In this chapter, we studied the spectroscopic properties of the ²⁶Mg nucleus using the PSDPF interaction, i.e. the energy spectrum and the strengths of the transitions in Weisskopf units (u.W.).
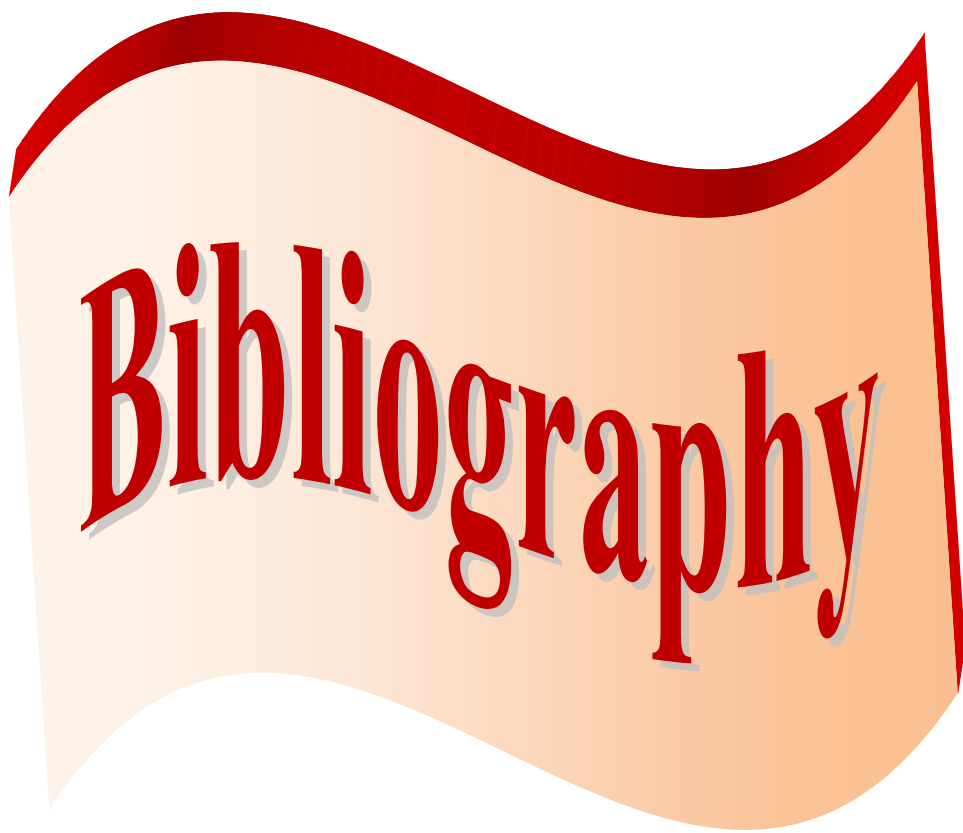
Conclusion

Conclusion

The aim of our work is the study of the spectroscopic properties of ^{26}Mg nucleus within the shell model framework. In the calculation, the Nathan code and the PSDPF interaction were used.

The energy spectrum of ^{26}Mg nucleus was calculated up to about 10 MeV. The PSDPF described quite well the reported properties. Through this study, we could get information about the collective states. This study allowed us also to confirm the uncertain states and to make important predictions of J^{π} Values for the ambiguous states. Them spin/parity assignments of all states in the ^{26}Mg nucleus constitute crucial indicators for identifying those in the mirror ^{26}Si nucleus, especially states of astrophysical interest.

The strengths of the transitions in Weisskopf units (u.W.) are a good test for any interaction. We calculated all the measured strengths and compared the to experiment. The results are in quite well agreement with experiment within the bar errors.

Bibliography

Bibliography

[1] A. Das , T. Ferbel,“ Introduction to Nuclear and particle physics”, University of Rochester, (2003).

[2] Johnson, K. E.“ From Natural History to the Nuclear Shell Model”,Lawrence University, (2004).

[3] M. Bouhelal, PhD Thesis, under joint supervision of University of Batna, Algeria and University of Strasbourg, France ,(2010).

[4] G. Fredrik , PhD Thesis , CERN, Arenberg Doctoral School,Faculty of Science,(2021)

[5] P. J. Brussaard, P. W. M. Glaudemans, “Shell–Model Applications in Nuclear Spectroscopy”, North–Holland, (1977).

[6] J. L. Basdevant, J. Rich, M. Spiro. p. cm.“Fundamentals in nuclear physics”,(2005)

[7] M. Alain GOASDUFF /Doctoral Thesis from the University of Strasbourg 2012

[8] R. R. Whitehead, A. Watt, B. J. Cole, I. Morrison, Adv. Nucl. Phys. 9, 123 (1977).

[9] E. Caurier, F. Nowacki, Acta Phys. Pol. B 30, 705 (1999).

[10] A. Schmidt et al, Phys. Rev. C 62, 044319 (2000).

[11] T. Mizusaki, RIKEN Accelerator Progress Report Vol. 33, 15 (2000).

[12] E. W. Ormand, C. W. Johnson, REDSTICK code, 2002.

[13] D. Zwarts, Comp, Phys, Comm. 38, 365 (1985).

[14] B. A. Brown et al., MSU–NSCL Report No. 524 (1985).

[15] A. Novoselsky, M. Vallières, Drexel University Shell–Model Code DUPSM (1997).

[16] E. Caurier et al., Phys. Rev. C 59, 2033 (1999).

[17] http://www.nndc.bnl.gov/nudat2

[18] B. H. Wildenthal, Prog. Part. Nucl. Phys. 11, 5 (1984).

[19] B. A. Brown, W. A. Richter, Phys. Rev., C 74, 034315 (2006).

[20] M. Bouhelal, F. Haas, E. Caurier, F. Nowacki, A. Bouldjedri, Nucl. Phys. A 864, 113 (2011)

[21] S. Aydin, M. Ionescu-Bujor, F. Recchia, A. Gadea, S.M. Lenzi, M. Bouhelal et al., DAE Symp. Nucl. Phys. 60, (2015) 94.

[22] S.Naima, B.Saadia, Master's Thesis, University of Tebessa, Algeria (2017).

[23] M. Bouhelal, F. Haas, E. Caurier, F. Nowacki,AIP Conf. Proc.1165, 61 (2009).

[24] M. Bouhelal, F. Haas, E. Caurier, F. Nowacki, Journal of Physics: Conference Series 580, 012025 (2015).

[25] M. Bouhelal, and F. Haas, Eur. Phys. J. Plus 131, 226 (2016).

[26] M. Bouhelal, M. Labidi, F. Haas, Few- Body Syst, Volume 58, Issue 2, article id.58, 4 pp (2017).

[27] M. Bouhelal, N. Azzeddine, N. Chorfi, F. Haas, Nuclear Theory, Vol. 37, 204 (2018), Heron Press, Sofia.

[28] M. Labidi, Master's Thesis, University of Tebessa, Algeria (2013).

[29] N. Chorfi, N. Azzeddine, Master's Thesis, University of Tebessa, Algeria (2017).

[30] M. Bouhelal, F. Haas, E. Caurier, F. Nowacki, AIP Conf. Proc.1491, 38 (2012).

[31] M. Abid, Master's Thesis, University of Tebessa, Algeria (2014).

[32] F. Drar, R. Bouchiba, Master's Thesis, University of Tebessa, Algeria (2017).

[33] H. Mebrek, M. Bouhelal, D. Bahloul, "Nuclear Theory" Vol. 38, 94 Heron Press, Sofia, (2019).

[34] H. Laidoudi, Master's Thesis, University of Tebessa, Algeria (2019) .

[35] A. Selim, K. Selim, Master's Thesis, University of Tebessa,Algeria (2020) .

[36] O. Ramdane, G. Fassekh, Master's Thesis, University of Tebessa, Algeria (2020).

[37] R. Mecheri, R. Doubia, Master's Thesis, University of Tebessa, Algeria (2021).

[38] M. R. Haouam, M. Bouhelal, F. Haas, E. Caurier, F. Nowacki, AIP Conf. Proc.1444, 375 (2012).

[39] M. R. Haouam, Master's Thesis, University of Tebessa, Algeria (2011).

[40] M. Bouhelal, F. Haas, E. Caurier, F. Nowacki, PoS (NIC XIII) 074 (2015), 5 pp., Proc. XIII Nuclei in the Cosmos (2014).

[41] M. Bouhelal, N. Saidane, S. Belaid, F. Haas, Can. J. Phys. 96 (7), 774 (2018).

[42] N. Saidane, S. Belaid, Master's Thesis, University of Tebessa, Algeria (2017).

[43] S. Aydin et al.,Phys. Rev. C 89, 014310 (2014).

[44] R. Chapman et al., Phys Rev C 93, 044318 (2016).

[45] R. Chapman et al., Phys Rev C 94, 024325 (2016).

[46] B. Fu et al., Phys Rev C 94, 034318 (2016).

[47] S. Aydin et al., Phys Rev C 96, 024315 (2017).

[48] R. Chapman et al., Phys Rev C 92, 044308 (2015).

[49] R. S. Lubna et al., Phys Rev C 97, 044312 (2018).

[50] L. Grocutt, R. Chapman , M. Bouhelal et al ., PhyRev C 100, 064308 (2019)

[51] Z. M. Wang et al.,Phys. Rev. C 81, 064301 (2010).

[52] S. Aydin et al.,Phys. Rev. C 86, 024320 (2012).

[53] S. Szilneret al.,Phys. Rev. C 87, 054322 (2013).

[54] S. Aydin, et al., Journal of Physics: ConferenceSeries 590, 012036 (2015).

[55] S. Szilner et al.,Phys. Rev. C 84, 014325 (2011).

[56] P. Marley et al.,Phys. Rev. C 84, 044332 (2011).

[57] D.G. Jenkins, M. Bouhelal, et al.,Phys. Rev. C 87, 064301 (2013).

[58] Z. Abla, A. Khaoula, Master's Thesis, University of Tebessa, Algeria (2022).

[59] M. Bouhelal, M. Labidi, F. Haas, E. Caurier, Phys. Rev. C 96, 044304 (2017).

[60] W. A. Richter, S. Mkhize, and B. Alex Brown, Phys. Rev. C 78, 064302 (2008).